Research Article Vol. 57, No. 6 / 20 February 2018 / Applied Optics 1321

applied optics

Measurement of multispecies concentration and gas temperature in an ammonium-dinitramide-based thruster by tunable diode lasers

Hui Zeng,[1,2] Fei Li,[2] Xilong Yu,[2,3,*] Dongbin Ou,[1] and Lianzhong Chen[1]

[1]China Academy of Aerospace Aerodynamics, Beijing Key Laboratory of Arc Plasma Application Equipment, Beijing 100074, China
[2]Key Laboratory of High Temperature Gas Dynamics, Institute of Mechanics, Chinese Academy of Sciences, Beijing 100190, China
[3]School of Engineering Science, University of Chinese Academy of Sciences, Beijing, China
*Corresponding author: xlyu@imech.ac.cn

Received 22 November 2017; revised 16 January 2018; accepted 18 January 2018; posted 19 January 2018 (Doc. ID 314064); published 14 February 2018

In this paper, quantitative experiments were made to measure the concentration of key intermediate products (CO, N_2O, and NO) and the gas temperature for combustion flow based on near-infrared and mid-infrared laser absorption spectroscopy. This paper used the developed diagnostic system to study two main ignition modes of a real 1-Newton thruster based on ammonium dinitramide (ADN): steady-state firing and pulse-mode firing over a feed pressure of 5–12 bar. The steady-state firing experiments distinguished the whole process into catalytic decomposition stage and combustion stage, experimentally demonstrating the combustion kinetics mechanism of an ADN monopropellant. Experiments for pulse-mode firing showed the measured multispecies concentration and temperature were consistent with pulse trains, verifying good performance for the thruster pulse-mode firing operation. The performance of the thruster was given based on the optical measurements, and characteristic velocity for the ADN-based thruster standard operation was higher than the corresponding 1-Newton hydrazine thruster.

OCIS codes: (140.2020) Diode lasers; (140.3600) Lasers, tunable; (280.1740) Combustion diagnostics; (280.4788) Optical sensing and sensors; (300.0300) Spectroscopy; (300.1030) Absorption.

https://doi.org/10.1364/AO.57.001321

1. INTRODUCTION

Recently, green space propulsion has become a common goal for small-satellite propulsion using nontoxic monopropellants, in which a new green liquid monopropellant based on ammonium dinitramide (ADN) has been developed for spacecraft propulsion [1]. Owing to higher performance, lower toxicity, and safer handling of the ADN monopropellant, an ADN-based thruster has great potential to replace the hydrazine thruster in small satellite missions. The development of an ADN liquid monopropellant for spacecraft propulsion has been discussed in previous studies [1–4]. ADN monopropellant is a liquid blend of high energetic oxidizing ADN ($NH_4N(NO_2)_2$), water, and fuel methanol [5]. Successful in-space demonstration of the high-performance green propulsion (HPGP) system based on a 1-N ADN-based thruster have been implemented on the PRISMA spacecraft platform [3,4,6,7]. However, the combustion mechanism of ADN monopropellant is not clear and is currently being studied theoretically. Most researchers divide the process of ADN monopropellant reactions into decomposition and combustion, and a mechanism has been proposed for decomposition reactions that involve two branches [8–11].

Figure 1 presents a brief scheme illustrating the decomposition and combustion process of an ADN monopropellant. Key reaction intermediates like N_2O and NO are generated by ADN decomposition and reduced by combustion, while CO stands for a typical products of methanol-related combustion reactions and represents the combustion degree. It is essential to better understand the combustion process of an ADN monopropellant by quantitatively measuring the flow parameters in a real ADN-based thruster to improve the performance of the thruster. Measurements of combustion parameters such as temperature and concentrations of key intermediates (N_2O, NO, and CO) provide access to quantitatively characterize the combustion process in the ADN-based thruster.

A new nonintrusive measurement system based on laser absorption spectroscopy is used for ADN combustion diagnostics and applied in this paper, while traditional diagnostic methods are disadvantageous for *in situ* measurements due to a long

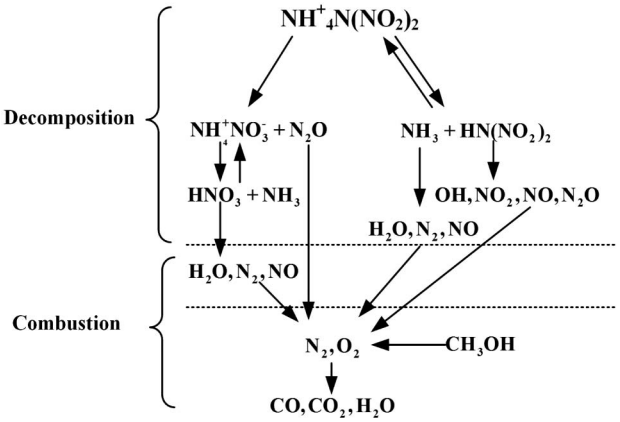

Fig. 1. Decomposition and combustion process of ADN monopropellant.

response time and intrusion into the flow field. The laser-based diagnostic system is developed by combining a mid-IR absorption sensor and near-IR absorption sensor to diagnose concentrations of key intermediates and gas temperature in the combustion chamber of a real ADN-based thruster during ground hot firing tests. Mid-IR quantum cascade laser (QCL) absorption spectroscopy is used to detect concentrations of N_2O, NO, and CO, while the gas temperature is measured by a near-IR diode absorption sensor. Preliminary measurements for N_2O concentration and gas temperature in a similar ADN-based thruster chamber have been presented in a previous work [12].

For concentration measurements, mid-IR laser diagnostics provide orders of magnitude greater detectivity, owing to much higher line strengths of transitions in mid-IR bands compared to near-IR bands, which offer higher signal-to-noise ratio (SNR) signals for accurate and precise concentration measurements for a small-sized thruster with an optical path length of 14 mm. A detailed review of developments in laser absorption spectroscopy using quantum cascade lasers (QCLAS) is presented in [13], and mid-IR QCLAS has been successfully applied in combustion diagnostics in variety of combustion facilities: Multispecies measurements of CO, CO_2, and H_2O are presented using mid-infrared absorption sensors within direct-connect model scramjet combustors [14,15]. CO concentration is measured using a mid-infrared absorption sensor at 4.8 μm in harsh, high-pressure combustion gases [16]. Measurements of NO have been reported in combustion exhaust gases of coal-fired power plants at temperatures up to 700 K at 5.2 μm [17].

For temperature measurements, near-IR H_2O two-line thermometry is a mature technique that has been applied for quantitative measurements of combustion flow in scramjets [18,19]. Near-IR H_2O two-line thermometry is suitable for high SNR measurements of combustion gas in an ADN-based thruster since more than 60% of the gas-mixture species is composed by water vapor in the chamber.

2. ABSORPTION SPECTROSCOPY

Laser absorption spectroscopy for molecular monochromatic transition at frequency v is expressed by the Beer–Lambert law, in which the relation between the transmitted intensity I_t through the gas medium of the optical path length L (cm) and the incident intensity I_0 can be expressed as

$$\frac{I_v}{I_0} = \exp(-\alpha_v), \tag{1}$$

where α_v represents the spectral absorbance coefficient. For an isolated transition,

$$\alpha_v = PXS(T)\phi(v - v_0)L, \tag{2}$$

where P (atm) is the pressure, X is the mole fraction of the target absorbing species, *and* $S(T)(\mathrm{cm^{-2}\,atm^{-1}})$ is the line strength of the transition at specific temperature $T(K)$. The temperature-dependent line strength can be expressed in terms of the known line strength at a reference temperature T_0 as

$$S(T) = S(T_0)\frac{Q(T_0)}{Q(T)}\left(\frac{T_0}{T}\right)\exp\left[-\frac{hcE''}{k}\left(\frac{1}{T} - \frac{1}{T_0}\right)\right] \times \left[1 - \exp\left(\frac{-hcv_0}{kT}\right)\right]\left[1 - \exp\left(\frac{-hcv_0}{kT_0}\right)\right]^{-1}, \tag{3}$$

where $Q(T)$ is the molecular partition function, $h(Js)$ is Planck's constant, c (cm/s) is the speed of light, k (J/K) is Boltzmann's constant, and E" $(\mathrm{cm^{-1}})$ is the lower-state energy. $\phi(v - v_0)$ (cm) is the line-shape function at the wavelength center of v_0. The line-shape function $\phi(v - v_0)$ is normalized such that $\int_{-\infty}^{+\infty}\phi(v - v_0)\mathrm{d}v = 1$ and the integrated absorbance $(\mathrm{cm^{-1}})$ can be expressed as

$$A = \int_{-\infty}^{+\infty}\alpha_v\mathrm{d}v = PXS(T)L. \tag{4}$$

Gas temperature can be obtained from the ratio of the two-line integrated absorbance area, and concentrations of the target species are acquired when P, $S(T)$, L are known by

$$T = \frac{\frac{hc}{k}(E_2'' - E_1'')}{\ln\frac{A_1}{A_2} + \ln\frac{S_2(T_0)}{S_1(T_0)} + \frac{hc}{k}\frac{(E_2'' - E_1'')}{T_0}} \quad X = \frac{A}{PS(T)L}, \tag{5}$$

3. LINE SELECTION

Tunable room-temperature, quantum-cascade, distributed-feedback lasers provide access to stronger transitions of N_2O, CO, and NO near 4.6 μm and 5.2 μm, respectively [20]. Since selected lines in mid-infrared bands are used for short optical path length, multispecies simultaneous measurement, wavelength selection for each species is mainly considered by line strength and isolation. Figure 2 gives line strengths of the primary species in combustion reactions of an ADN monopropellant over the range 1–6 μm at a temperature of 1000 K.

A. Line Selection for Temperature Measurement

Line selection criteria for H_2O two-line thermometry has been discussed in previous work [22], and transitions of water vapor used in this work is presented in Table 1. The two selected H_2O lines with well-known parameters have been applied to temperature measurements for a variety of harsh combustion environments reported in [18,23,24]. In this work, interference

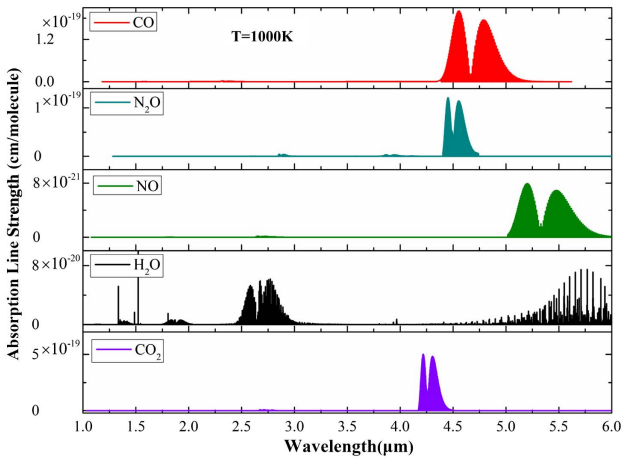

Fig. 2. Transition line strengths in 1–6 μm for CO, N_2O, NO, H_2O, and CO_2 at 1000 K from HITRAN [21].

Table 1. Spectroscopic Line Parameters for Species Temperature Measurements [21]

Line	Line-Center Wavelength (cm^{-1})	Line Strength S (296 K) (cm^{-2} atm^{-1})	Lower State Energy E'' (cm^{-1})
1	7185.597	0.0197	1045.058
2	7444.35 + 7444.37 (combined)	0.00112	1774.751 1806.670

from other species transitions, like CO, CO_2, N_2O, and NO, can be negligible since line strengths of these species transitions are at least two orders of magnitude lower than the line strengths of H_2O transitions near 7185 cm^{-1} and 7444 cm^{-1}. Meanwhile, the H_2O two-line thermometry is highly sensitive to temperature over the thruster operation temperature of 400–1600 K, and the temperature can be obtained from the ratio of the measured integrated absorbance of two transitions, as shown in Fig. 3.

B. Line Selection for Species Concentration Measurement

Figure 4 presents spectrum absorbance simulation near 4.6 μm and 5.2 μm for the multispecies of H_2O, CO, CO_2, N_2O, and NO, of which the composition is approximately 60% for H_2O and 5% for the four other species, respectively. As noted in Fig. 4(a), transitions spectral absorbance of N_2O and CO is high and suitable for measurements with negligible spectral absorbance for other species in the wavelength region of 2187 cm^{-1}–2201 cm^{-1} near 4.6 μm. The strong absorption of N_2O and CO is partially overlapped, which is useful for simultaneous detection of N_2O and CO in a single period scan, and two N_2O transitions centered at 2192.48 and 2193.54 cm^{-1} and one CO transition centered at 2193.36 cm^{-1} are chosen (Table 2). To infer mole fraction of the species, a multipeak fitting strategy is used, which has been reported in [25–27]. Except for interferences from transitions of water vapor,

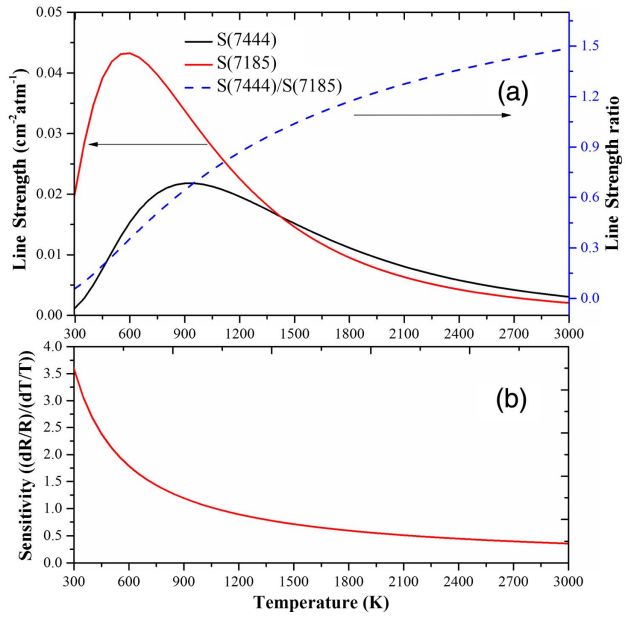

Fig. 3. Temperature sensing parameters for H_2O transitions line pair. (a) Line strength and the ratio versus temperature and (b) line strength ratio sensitivity versus temperature.

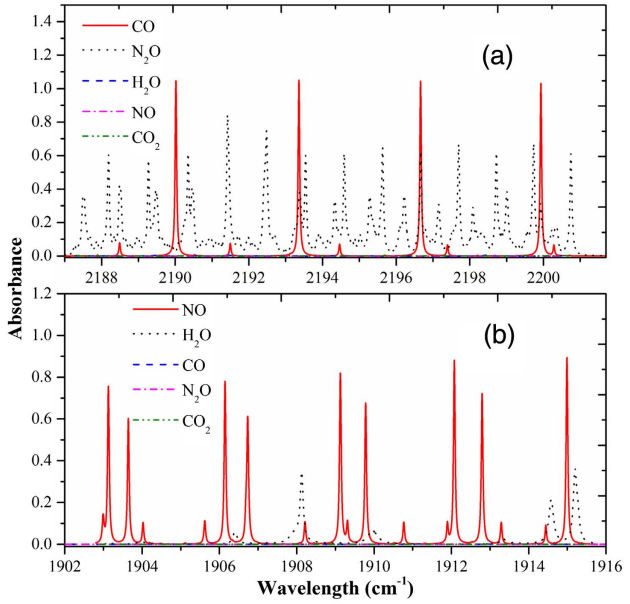

Fig. 4. Spectrum simulation from HITRAN in the laser operation range near: (a) 4.6 μm; and (b) 5.2 μm. $P = 1$ atm, $T = 1000$ K, $L = 1$ cm, $X_{CO} = 0.05$, $X_{N_2O} = 0.05$, $X_{H_2O} = 0.6$, $X_{NO} = 0.05$, $X_{CO_2} = 0.05$.

the spectrum simulation of Fig. 4(b) shows that the spectral absorbance of NO is strong and has no interference by other species in the wavelength region of 1902 cm^{-1}–1916 cm^{-1} near 5.2 μm. A NO transition centered at 1912.07 cm^{-1} is used to minimize the interference of water vapor transitions.

Table 2. Spectroscopic Line Parameters for Species Concentration Measurements [21]

Species	Line-Center Wavelength v_0 (cm^{-1})	Line Strength S (296 K) (cm^{-2} atm^{-1})	Lower State Energy E'' (cm^{-1})
N_2O	2192.48	8.39	469.91
N_2O	2193.54	9.30	442.28
CO	2193.36	6.02	349.70
NO	1912.07	2.64	200.63

4. EXPERIMENTAL SETUP

A. Thruster Characterization and Scheme for Optical Arrangement

Measurements were conducted on a 1-Newton ADN-based thruster, as shown in Fig. 5. The experimental ADN thruster was composed of a solenoid valve, injector, catalyst bed, combustion chamber, and nozzle. The catalyst bed was filling with a grain-type catalyst coating iridium as an active component. A sheathed heater was attached to the outer wall of the catalyst bed, and it preheated the catalyst to initiate the decomposition of ADN. The ADN liquid monopropellant was composed of 61% ADN, 27% water, and 12% methanol by mass. When the thruster operated, the liquid propellant was driven by pressurized nitrogen and atomized into droplets by the injector, gasified, and catalytically decomposed into gaseous intermediates by preheated catalyst particles in the catalytic bed, and small-molecule intermediates reacted in the combustion chamber and discharged through the nozzle. The ADN-based thruster was operated under two standard conditions: steady-state firing and pulse-mode firing. In the present experiments, steady-state firing was performed at a duration of 10 s and pulse-mode firing was conducted at pulse duration of 100 ms ON to 2 s OFF for 10 pulse trains operation. Hot firing tests were carried out over a feed-pressure range of 5–12 bar at an ignition temperature of 200°C.

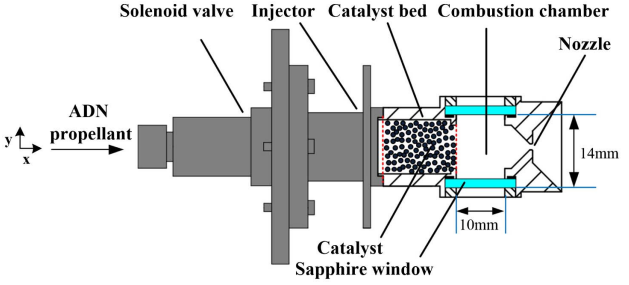

Fig. 5. Schematic of the ADN thruster.

For optical measurements, two sapphire windows with 12.7 mm in diameter were installed in the sidewalls of the combustion chamber with a 10 mm × 3.5 mm effective light area, and the combustion chamber was manufactured with a thicker wall for optical window implementation, as shown in Fig. 5. All windows were wedged with 3° on the outer face to avoid interference from internal etalon-type reflections as laser beams passed through. A pressure tap was drilled with diameter of 0.7 mm in the top wall of the combustion chamber for combustion pressure monitoring.

B. Laser-Based Absorption Diagnostic System

Figure 6 presents the layout of the laser-based absorption diagnostic system in this study. Optical measurements for the ADN-based thruster confronted challenges due to its small combustion chamber with an optical path length of 14 mm, which required a cautious optical layout. Two distributed-feedback (DFB) quantum cascade lasers (Alpes Lasers, Neuchatel, Switzerland) were used: one laser near 4.6 μm for simultaneous N_2O and CO measurements and another laser near 5.2 μm for NO measurement, respectively. Meanwhile, two DFB InGaAsP lasers (NEL NLK1B5EAAA, Yokohama, Japan) were used to monitor water vapor transitions in near-IR. Scanned-wavelength direct absorption is used to target the transitions, while wavelength modulation spectroscopy is not applicable here because of inaccurate broadening coefficients associating with such high pressures and complex components composition in the combustion chamber of the ADN-based thruster.

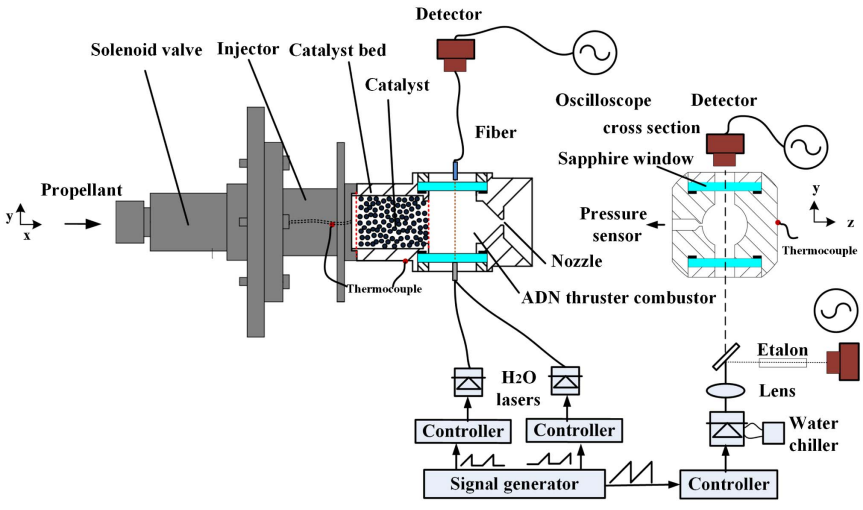

Fig. 6. Laser-based absorption sensor layout.

For concentration measurements, the output of the quantum cascade laser was tuned by changing the temperature of the laser chip and injection current, which were modulated by Alpes Lasers TC-3 and ILX Lightwave LDX-3232 (ILX Lightwave, Bozeman, Montana, USA), respectively, while a pump-driven water chiller was used to cool the laser device. The laser wavelength was scanned over the entire absorption feature of the target transitions by injection current using a sawtooth signal at a frequency of 100 Hz and a constant tuning temperature. Collimated output of the laser was divided into two beams by a splitter. One beam was transmitted through the combustion chamber, focused by a lens, then passed through a filter, and finally detected by a liquid nitrogen-cooled InSb detector (Infrared Associates, Inc., Stuart, Florida, USA). The second beam was propagated through a silicon etalon (LightMachinery, Inc., Ottawa, Ontario, Canada) with a free spectral range (FSR) of 0.018 cm^{-1} to provide calibration between time domain and wavelength domain and detected by another InSb detector.

The temperature sensor consisted of two distributed-feedback tunable diode lasers (TDL) emitting near 1343 nm and 1392 nm. The two diode lasers temperature and injection current were modulated by two diode-laser controllers (ITC4001, Thorlabs, Newton, New Jersey, USA), respectively. The laser wavelength was tuned using a ramp with frequency of 1 kHz via a time division multiplexing (TDM) strategy. A 2 mm diameter fiber-coupled collimator was used to ensure that the multilights were passing through the optical path closely. The transmitted signals were collected by a multimode fiber and then detected by an InGaAs detector. The optics and detector were situated close to the window and were purged with nitrogen to remove any interfering absorption by ambient water vapor. A measured position was installed at the center of the combustion chamber along the axis. Additional measurement of combustion pressure was carried out using a high frequency pressure sensor (CYG1508 series, Kunshan Bridging Sensor Control Technology Co., Ltd., Kushan, China) with a response frequency of 20 kHz. All detector signals were acquired by oscilloscopes (DPO3034, Tektronix, Beaverton, Oregon, USA).

Laser-based absorption measurements were path integrated in nature. Therefore, if the optical path exhibited nonuniformity in terms of temperature and/or concentration, the LAS measurements yielded average values for temperature and concentration. A previous study had been aimed at quantifying nonuniformity for path-averaged measurements [28]. Based on previous work, the measured cross section of the ADN-based thruster employed in the present study showed that thermal boundary-layer thickness versus optical path length was 2.2%, leading to a 4.3% variation in temperature measurements and 0.8% variation in concentration measurements; thus, a cross section of the combustion chamber was quasi-uniform, and combustion of the ADN monopropellant was assumed to be a quasi-one-dimensional flow along the axial direction.

5. RESULTS AND DISCUSSION

A. Measurements for Steady-State Firing

Measurements for steady-state hot firing were performed for a 10 s duration at a ignition temperature of 200°C and over a feed pressure range of 5–12 bar, in which feed pressure of 12 bar corresponded to standard operation for the thruster. The 4.6 μm quantum cascade laser was first used to measure N_2O and CO, and then the 5.2 μm laser was installed for NO measurement, while other sensor kept operating, as shown in Fig. 6. All experiments were conducted under the same operating condition in the same day. As shown in Fig. 7, measurements of the combustion pressure were always conducted and the measured pressure trace showed great consistency in different runs under the same operating conditions, indicating that the thruster operation was highly repeatable, which allowed direct comparison between the two QCL sensors results. It should be noted that the combustion pressures showed a little difference in the beginning in two runs under a feed pressure of 12 bar. The reason was that one of the tests was the first firing for the cold thruster and the measured pressure showed slower equilibrium.

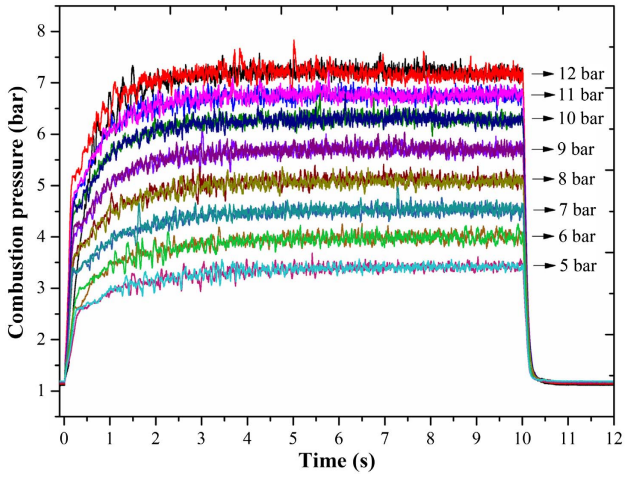

Fig. 7. Measured pressure in the combustion chamber for steady-state firing.

As the thruster firing initiated, the combustion pressure rapidly increased and reached equilibrium until the firing ended, indicating a stable heat release from the ADN monopropellant combustion. Equilibrium values of the combustion pressure for the steady-state firing decreased linearly and the corresponding equilibrium time increased when the feed pressure gradually decreased, as shown in Fig. 8.

Figure 9 presents the measured concentration of N_2O, NO, and CO for 10 s steady-state firing under the thruster operating conditions. Concentrations of N_2O and NO increased, indicating rapidly decomposition of ADN synchronizing with the thruster operation. Then N_2O and NO values decreased and reached equilibrium at levels close to zero. As methanol-related combustion went on, mole fraction of CO gradually increased and was partially oxidized to CO_2, reaching equilibrium at levels of 3–6%. The equilibrium moments of N_2O, NO, and CO concentration showed great consistency. Compared to the N_2O and CO measurements, CO slowly increased while N_2O rapidly increased in the early period of firing, implying that methanol-related combustions were slower than decomposition of ADN.

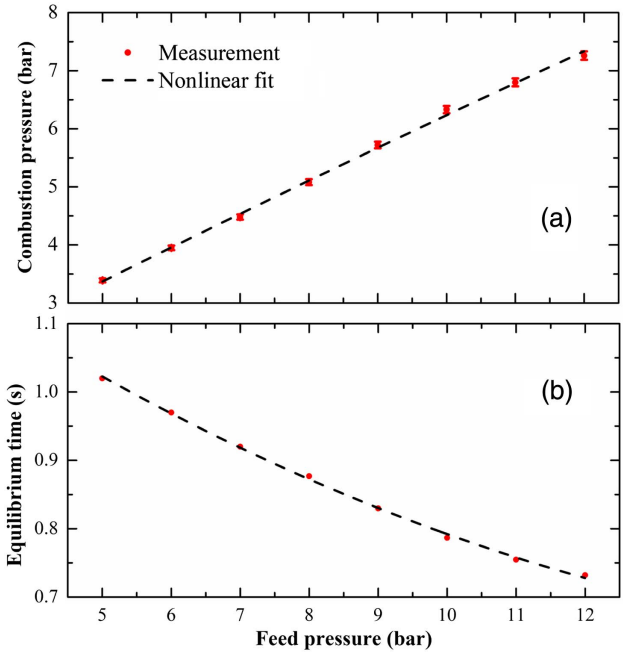

Fig. 8. Combustion pressure versus feed pressure for steady-state firing. (a) Equilibrium steady-state value and (b) equilibrium time.

For N_2O measurements in the first 2 s firing, increase and decrease of N_2O clearly identify ADN decomposition and methanol-related combustion, respectively. The reaction rates of decomposition and combustion decreased and the moments of the peak N_2O concentration increased as the feed pressure decreased from 12 bar to 5 bar, leading to a slower heat release and lower combustion pressure, corresponding to the results in Fig. 8. Similar trends of measured NO and CO were found as the thruster operated over the feed-pressure range. The peak NO concentration decreased as the feed pressure dropped,

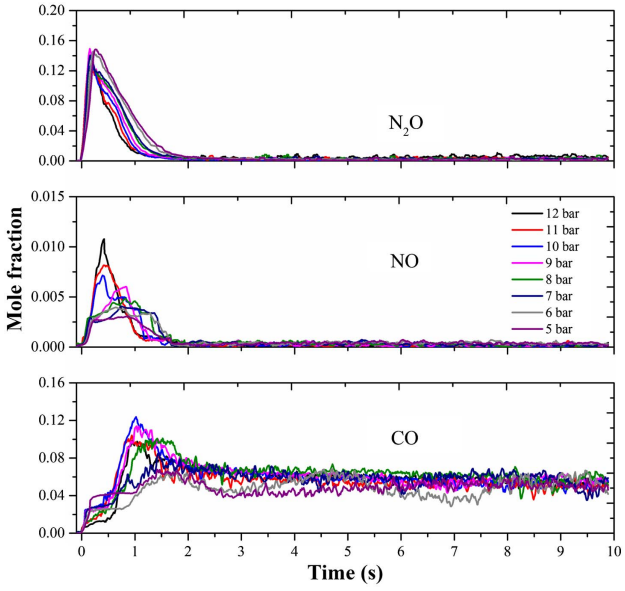

Fig. 9. Measured concentration of N_2O, NO, and CO in the combustion chamber for steady-state firing.

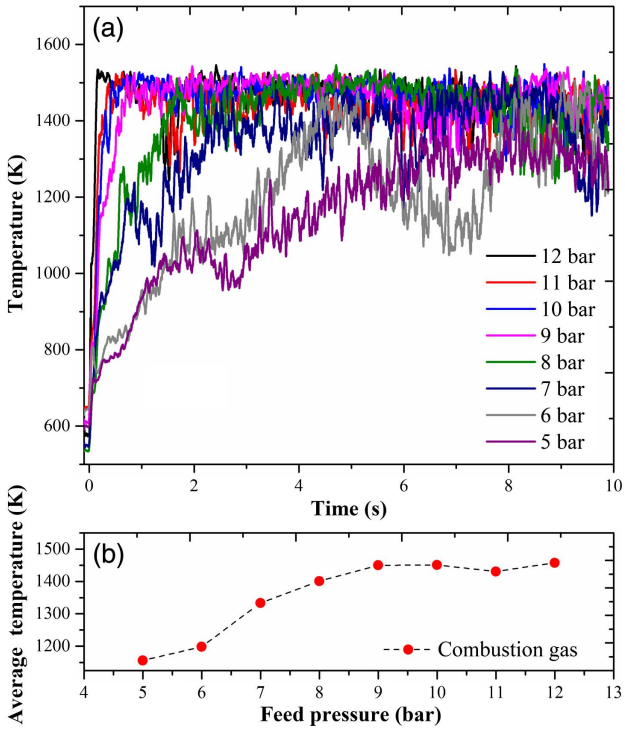

Fig. 10. Measured temperature in the combustion chamber for steady-state firing. (a) Temperature versus 10 s firing and (b) average temperature versus feed pressure.

while the peak CO concentration maintained stable at levels of 10%–12% over the feed pressure of 8–12 bar and fell to below 8% over a feed pressure of 5–7 bar.

Results of the gas temperature in the combustion chamber for steady-state firing are shown in Fig. 10(a). For the thruster standard operation, the combustion temperature rapidly increased and reached equilibrium with a value of nearly 1500 K. For comparison, the experimentally determined temperature for pure ADN combustion at 0.5 MPa was 1350 K [10], and the numerical result for the equilibrium temperature in the combustion chamber when operating an ADN monopropellant thruster was nearly 1600 K [29]. The thruster chamber wall temperature ranged from 1100°C to 1480°C during steady-state firing in the HPGP thruster developed by ECAPS [7].

As the feed pressure decreased, slower equilibrium of the combustion temperature was obtained, following with a larger vibration. The results demonstrated transition from combustion stability to combustion instability for a 10 s thruster operation and indicated a worse performance of the thruster. Figure 10(b) gives the average value of the gas temperature during the 10 s operation under different feed pressure. Over the feed pressure range of 9–12 bar, the average temperature kept at nearly 1450 K, indicating stable combustion for the thruster operation. Then the average temperature decreased sharply from 1400 K to 1150 K as the feed pressure further decreased below 8 bar, illustrating incomplete combustion reactions of the monopropellant in the chamber and bad performance of the thruster. For stable and normal operation of the thruster, the threshold of feed pressure should be more than 8 bar.

B. Measurements for Pulse-Mode Firing

Measurements for pulse-mode firing were conducted for 10 pulse trains operation (100 ms ON and 2 s OFF). Figure 11 gives the measured results of the combustion pressure under the feed-pressure operation conditions. The combustion pressure sharply increased as the pulse firing initiated and decreased as the pulse firing ended, showing good consistency with the pulse trains and indicating great performance for the thruster pulse-mode operation. As the pulse trains carried on, the maximum pressure values during one pulse operation gradually increased, which were lower than the corresponding values for steady-state firing. For the last pulse operation, as shown in the enlargement of Fig. 11, the combustion pressure decreased as the feed pressure dropped.

Figure 12 presents the measured concentration of N_2O, NO, and CO for pulse-mode firing under the feed-pressure operation conditions. As a pulse firing ended, the multispecies values slowly decreased for the first few pulses firing, then the rates of multispecies values were gradually increased and the characteristic of the multispecies concentration was consistent with the pulse trains as the pulse firing carried on. Under more pulse-trains firing, the measured multispecies concentration indicated an increasing degree of reactions and better performance for the thruster pulse-mode operation.

For N_2O and NO measurements, the maximum values of the two species in each pulse decreased as the pulse trains carried on, implying increasing combustion reactions. Incomplete combustion was obtained as the maximum CO of each pulse varied over 2%–8% for 10 pulse trains operation. Before the firing ended, the maximum value of N_2O concentration increased as the feed pressure decreased for the last pulse train, as shown in Fig. 12(b). The measurements demonstrated a slower degree of decomposition and combustion of the ADN monopropellant when the feed pressure went down.

Figure 13 shows the measured temperature in the combustion for 10 pulse trains firing, showing good consistency with the measured pressure and pulse trains. The maximum values of gas temperature during each pulse operation were irregularly varied under different feed-pressure operations. It should be noted that the temperature vibration directed by the arrow in Fig. 13 was not in coincidence with the real combustion situation, in which the combustion temperature should be stable. This happened because unreacted gas-liquid phase products contaminated the sapphire window and interfered with the optical measurement when a laser beam was just passing through.

Measurement uncertainty of LAS diagnostics was carefully evaluated in the temperature and concentration measurements. For uncertainty evaluation of temperature measurements, measurement uncertainty in temperature relied on the uncertainty of integrated area measurements, according to Eq. (5). In our measurements, Voigt fitting was conducted to process the raw absorption signals and a maximum fitting error of 0.8% was obtained in integrated area measurements, translating into 1.6% error in the ratio of the integrated absorbance between two transitions. Considering a maximum 4.3% variation in temperature measurements caused by temperature nonuniformity in previous work [12], measurement uncertainty of temperature was nearly 4.6%. For uncertainty evaluation of concentration measurements, laboratory calibration was conducted by using the developed mid-IR laser senor in a high-pressure cell capable of gas pressures up to 10 atm and temperatures up to 700 K. The maximum error for concentration measurements was nearly 8%, considering a 1% uncertainty in pressure measurements and a 2% uncertainty in optical path length determination.

C. Performance Evaluation of the Thruster

The characteristic velocity measures the effectiveness of the combustion. A common method to evaluate the performance of thruster is given in [30], and can be expressed as

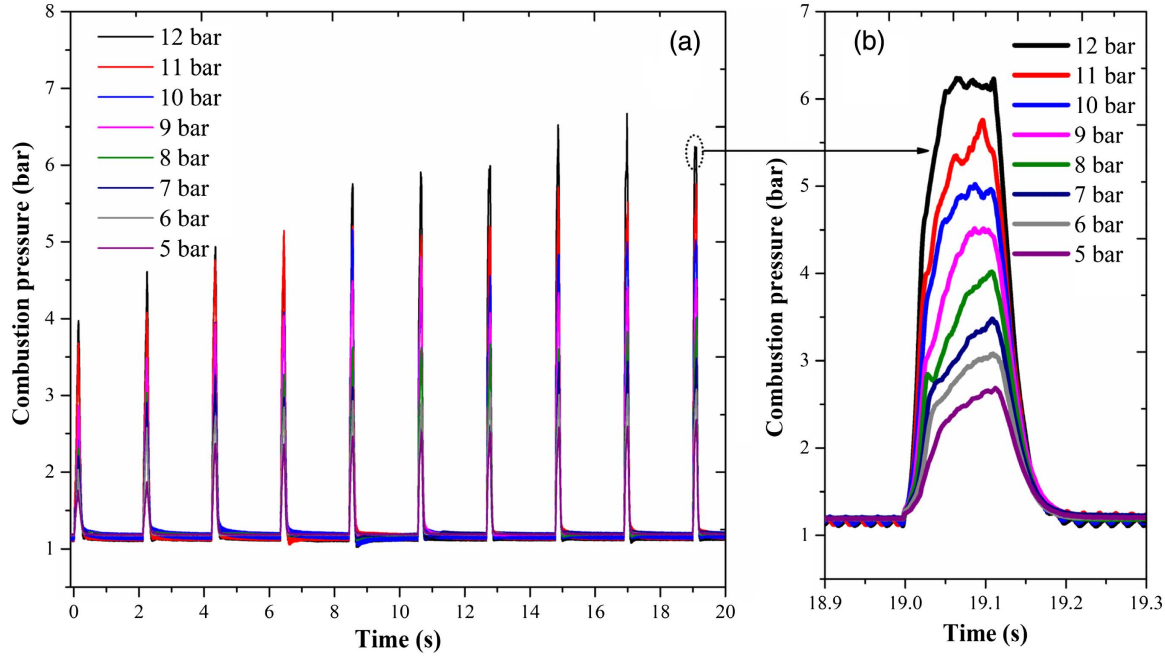

Fig. 11. Measured pressure in the combustion chamber for pulse-mode firing.

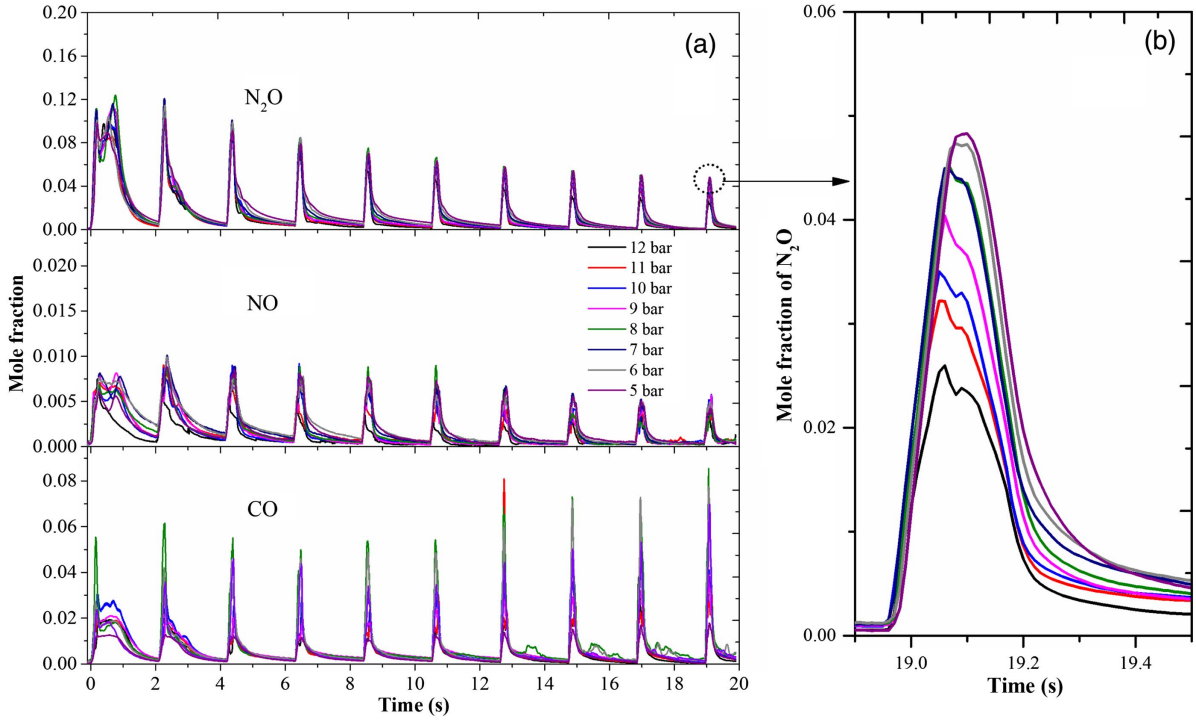

Fig. 12. Measured concentration of N_2O, NO, and CO in the combustion chamber for pulse-mode firing.

$$C^* = \frac{\sqrt{\gamma R T_c}}{\gamma\sqrt{\left(\frac{2}{\gamma+1}\right)^{\frac{\gamma+1}{\gamma-1}}}},$$

where T_c is the gas temperature in the combustion chamber and γ is the specific heat ratio. The value of the specific heat ratio equals the weighted values of the combustion products (H_2O, N_2, N_2O, CO, and NO) at various temperatures [28].

Figure 14 gives the characteristic velocity based on the measurements of species concentrations and temperature for steady-state and pulse-mode firing. The values for pulse-mode firing were calculated according to measurements during the last pulse operation. The characteristic velocity increased as the feed pressure increased, maintained over 1050–1150 m/s for steady-state firing and 850–1050 m/s, respectively. The characteristic velocity value of 1150 m/s for standard steady-state firing was higher than the 1-Newton hydrazine thruster with a characteristic velocity value of less than 1100 m/s, demonstrating better performance for the 1-Newton ADN-based thruster. For uncertainty analysis, the characteristic velocity relied on the measurements of gas temperature and concentration using LAS technique. Measurement uncertainty in temperature measurements was 4.6%, while uncertainty in concentration

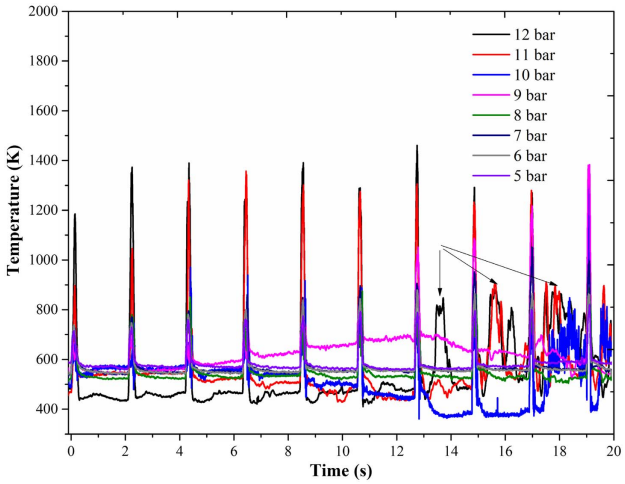

Fig. 13. Measured temperature in the combustion chamber for pulse-mode firing.

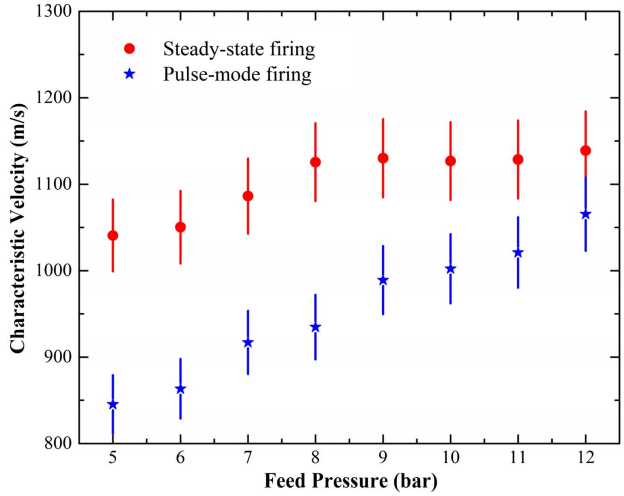

Fig. 14. Characteristic velocity for steady-state firing and pulse-mode firing.

measurements was 8%. Over the combustion temperature range from 300 K to 1500 K and a combustion pressure range from 2 bar to 7 bar, the specific heat ratio γ was less sensitive to a variation in temperature/pressure [28]. Thus, the uncertainty of a specific heat ratio for combustion gases in the chamber was 8% contributing by concentration measurements. According to Eq. (4), the uncertainty of characteristic velocity was 4.2%.

6. CONCLUSION

Simultaneous laser-based absorption measurements of N_2O, CO, NO, and gas temperature were performed in a small-sized ADN-based thruster employing mid-IR quantum cascade lasers and near-IR diode lasers. *In situ* measurements were conducted in the center cross section of the combustion chamber under the feed-pressure operation conditions for both steady-state firing and pulse-mode firing. Time-resolved results provided quantitative information to gain insight into the combustion process inside the thruster and clarify the decomposition of ADN and methanol-related combustions. Measurements for steady-state firing showed that the measured increase and decrease of N_2O represented the reaction rates of decomposition and combustion, which decreased as the feed pressure dropped, corresponding to decreasing combustion pressure. Moreover, there existed a pressure lower-limit threshold (>8 bar) for the thruster normal operation based on the temperature results. Measured results of multispecies concentrations and gas temperature for pulse-mode firing were consistent with the pulse trains. According to the N_2O measurements, increasing decomposition of ADN was found as the feed pressure increased and the combustion reaction rate gradually increased as pulse trains carried on, indicating incomplete equilibrium for 10 pulse trains operation. Performance of the thruster was given based on the optical measurements, and characteristic velocity for the ADN-based thruster standard operation was higher than the corresponding 1-Newton hydrazine thruster. The laser-based absorption sensor demonstrated its capability for small-sized thruster applications and could be used as a normal combustion diagnostic technique for thruster hot firing tests.

Funding. National Natural Science Foundation of China (NSFC) (11372329, 90816015).

REFERENCES

1. A. S. Gohardani, J. Stanojev, A. Demaire, K. Anflo, M. Persson, N. Wingborg, and C. Nilsson, "Green space propulsion: opportunities and prospects," Prog. Aerosp. Sci. **71**, 128–149 (2014).
2. K. Anflo, T.-A. Grönland, G. Bergman, M. Johansson, and R. Nedar, "Towards green propulsion for spacecraft with ADN-based monopropellants," in *38 th AIAA Joint Propulsion Conference* (AIAA Paper, 2002), Vol. **3847**, p. 2002.
3. M. Lange, A. Lein, U. Gotzig, T. Ziegler, S. Anthoine, M. Persson, and K. Anflo, "Introduction of a high-performance ADN based monopropellant thruster on the Myriade propulsion subsystem technical and operational concept and impacts," in *6th International Conference on Recent Advances in Space Technologies (RAST)* (IEEE, 2013), pp. 549–553.
4. K. Anflo and R. Mollerberg, "Flight demonstration of new thruster and green propellant technology on the PRISMA satellite," Acta Astronaut. **65**, 1238–1249 (2009).
5. A. Larsson and N. Wingborg, "Green propellants based on ammonium dinitramide (ADN)," in *Advances in Spacecraft Technologies* (2011), pp. 139–156.
6. K. Anflo and B. Crowe, "In-space demonstration of an ADN-based propulsion system," in *47th AIAA/ASME/SAE/ASEE Joint Propulsion Conference & Exhibit* (American Institute of Aeronautics and Astronautics, 2011).
7. P. Nils, A. Kjell, and S. Oskar, "Spacecraft system level design with regards to incorporation of a new green propulsion system," in *47th AIAA/ASME/SAE/ASEE Joint Propulsion Conference & Exhibit* (American Institute of Aeronautics and Astronautics, 2011).
8. S. Vyazovkin and C. A. Wight, "Ammonium dinitramide: kinetics and mechanism of thermal decomposition," J. Phys. Chem. A **101**, 5653–5658 (1997).
9. J. C. Bottaro, P. E. Penwell, and R. J. Schmitt, "1, 1, 3, 3-tetraoxo-1, 2, 3-triazapropene anion, a new oxy anion of nitrogen: the dinitramide anion and its salts," J. Am. Chem. Soc. **119**, 9405–9410 (1997).
10. V. P. Sinditskii, V. Y. Egorshev, A. I. Levshenkov, and V. Serushkin, "Combustion of ammonium dinitramide, part 2: combustion mechanism," J. Propul. Power **22**, 777–785 (2006).
11. O. P. Korobeinichev, T. A. Bolshova, and A. A. Paletsky, "Modeling the chemical reactions of ammonium dinitramide (ADN) in a flame," Combust. Flame **126**, 1516–1523 (2001).
12. H. Zeng, F. Li, S. Zhang, X. Yu, W. Zhang, and Z. Yao, "Midinfrared absorption measurements of nitrous oxide in ammonium dinitramide monopropellant thruster," J. Propul. Power **31**, 1496–1500 (2015).
13. L. Zhang, G. Tian, and B. Yu, "Applications of absorption spectroscopy using quantum cascade lasers," Appl. Spectrosc. **68**, 1095–1107 (2014).
14. I. A. Schultz, C. S. Goldenstein, R. M. Spearrin, J. B. Jeffries, R. K. Hanson, R. D. Rockwell, and C. P. Goyne, "Multispecies midinfrared absorption measurements in a hydrocarbon-fueled scramjet combustor," J. Propul. Power **30**, 1595–1604 (2014).
15. R. Spearrin, C. Goldenstein, I. Schultz, J. Jeffries, and R. Hanson, "Simultaneous sensing of temperature, CO, and CO_2 in a scramjet combustor using quantum cascade laser absorption spectroscopy," Appl. Phys. B **117**, 689–698 (2014).
16. R. Spearrin, C. Goldenstein, J. Jeffries, and R. Hanson, "Quantum cascade laser absorption sensor for carbon monoxide in high-pressure gases using wavelength modulation spectroscopy," Appl. Opt. **53**, 1938–1946 (2014).
17. X. Chao, J. B. Jeffries, and R. K. Hanson, "In situ absorption sensor for NO in combustion gases with a 5.2 μm quantum-cascade laser," Proc. Combust. Inst. **33**, 725–733 (2011).
18. F. Li, X. L. Yu, H. B. Gu, Z. Li, Y. Zhao, L. Ma, L. H. Chen, and X. Y. Chang, "Simultaneous measurements of multiple flow parameters for scramjet characterization using tunable diode-laser sensors," Appl. Opt. **50**, 6697–6707 (2011).
19. F. Li, X. Yu, W. Cai, and L. Ma, "Uncertainty in velocity measurement based on diode-laser absorption in nonuniform flows," Appl. Opt. **51**, 4788–4797 (2012).
20. K. Namjou, S. Cai, E. Whittaker, J. Faist, C. Gmachl, F. Capasso, D. Sivco, and A. Cho, "Sensitive absorption spectroscopy with a room-temperature distributed-feedback quantum-cascade laser," Opt. Lett. **23**, 219–221 (1998).
21. L. Rothman, I. Gordon, Y. Babikov, A. Barbe, D. C. Benner, P. Bernath, M. Birk, L. Bizzocchi, V. Boudon, and L. Brown, "The HITRAN2012 molecular spectroscopic database," J. Quantum Spectrosc. Radiat. Transfer **130**, 4–50 (2013).
22. X. Zhou, X. Liu, J. B. Jeffries, and R. K. Hanson, "Development of a sensor for temperature and water concentration in combustion gases using a single tunable diode laser," Meas. Sci. Technol. **14**, 1459–1468 (2003).
23. J. T. Liu, G. B. Rieker, J. B. Jeffries, M. R. Gruber, C. D. Carter, T. Mathur, and R. K. Hanson, "Near-infrared diode laser absorption diagnostic for temperature and water vapor in a scramjet combustor," Appl. Opt. **44**, 6701–6711 (2005).
24. S. T. Sanders, J. A. Baldwin, T. P. Jenkins, D. S. Baer, and R. K. Hanson, "Diode-laser sensor for monitoring multiple combustion parameters in pulse detonation engines," Proc. Combust. Inst. **28**, 587–594 (2000).

25. X. Liu, J. Jeffries, R. Hanson, K. Hinckley, and M. Woodmansee, "Development of a tunable diode laser sensor for measurements of gas turbine exhaust temperature," Appl. Phys. B **82**, 469–478 (2006).
26. S. Wagner, B. T. Fisher, J. W. Fleming, and V. Ebert, "TDLAS-based in situ measurement of absolute acetylene concentrations in laminar 2D diffusion flames," Proc. Combust. Inst. **32**, 839–846 (2009).
27. C. D. Lindstrom, D. Davis, S. Williams, and C.-J. Tam, "Shock-train structure resolved with absorption spectroscopy part II: analysis and CFD comparison," AIAA J. **47**, 2379–2390 (2009).
28. R. W. Fox, A. T. McDonald, and P. J. Pritchard, *Introduction to Fluid Mechanics* (Wiley, 1985).
29. T. Zhang, G. X. Li, Y. S. Yu, Z. Y. Sun, M. Wang, and J. Chen, "Numerical simulation of ammonium dinitramide (ADN)-based non-toxic aerospace propellant decomposition and combustion in a monopropellant thruster," Energy Convers. Manage. **87**, 965–974 (2014).
30. O. E. Lancaster and T. von Kármán, *Jet Propulsion Engines* (Princeton University, 1959).